Proceedings of ICRC 2001: 2575 © Copernicus Gesellschaft 2001

ICRC 2001

VHE observations of unidentified EGRET sources

S. J. Fegan[1,2]**, T. C. Weekes**[1]**, and the VERITAS collaboration**[1]

[1]Fred Lawrence Whipple Observatory, PO Box 97, Amado, AZ 85645, USA
[2]Physics Department, University of Arizona, Tucson, AZ 85721, USA

Abstract. Observations of unidentified EGRET sources were made with the Whipple 10m imaging atmospheric Čerenkov telescope between Fall 1999 and Spring 2001. During this period, a high resolution 490 pixel camera with 4° field of view was present on the telescope. Characterization of the off-axis response of this instrument was done using observations of the Crab Nebula. No significant emission was detected from the eight unidentified EGRET sources observed and upper limits are presented as a function of position.

1 Introduction

Very High Energy (VHE) γ-ray astronomy is the term used to describe observations in the energy range from 300GeV to 100TeV. Ground-based instruments operating in this energy domain typically have large collecting areas, good angular resolution and relatively large fields of view. The atmospheric Čerenkov imaging technique is described in detail elsewhere (Ong, 1998). Its fundamental challenge is to infer the composition, energy and arrival direction of a primary γ-ray from the image of its induced particle air shower.

Twenty five years of gamma ray observations in the MeV to GeV range, have produced nearly 300 cataloged sources. During its lifetime, the EGRET experiment aboard CGRO made the most significant contribution to the list of detected sources, although its relative insensitivity to the arrival direction of 100 MeV photons means that the location of many sources are only known to within $\sim 0.5^\circ$.

At high galactic latitude many of the sources detected by EGRET have been associated with blazars, a class of AGN. At low galactic latitude ($b < 10^\circ$) 7 or 8 sources have been associated with young pulsars. The majority of sources are, as yet, not firmly associated with objects at other wavelengths. In many cases the EGRET error circle is populated by a number of prospective X-ray, optical and radio sources which are all candidate associations.

Correspondence to: T. C. Weekes
(tweekes@cfa.harvard.edu)

2 Observations

Observations of eight unidentified EGRET sources were made with the Whipple 10m imaging atmospheric Čerenkov telescope in Arizona USA. The instrument and its characteristics are described in Finley et al. (2001). The camera consists of 379 0.118° PMTs in a close packed arrangement and an outer section of 111 0.23° PMTs arranged in three rings. Only data from the inner 379 channels are used here.

Data taking at the Whipple 10m telescope is arranged into seasons broken by the summer monsoon period, which is usually used to make improvements to the instrument. Data presented here are from two such seasons, Fall 1999–Summer 2000 and Fall 2000–Summer 2001. Mirror recoating that took place during the end of the first season and the intervening summer led to a higher sensitivity during the 2000/2001 season.

For off-axis and extended sources the telescope is operated in ON-OFF mode. Each 28 minute scan of the source region is followed by a 28 minute control run offset from the source by 30 minutes in right ascension and in time. Taking the control data in this manner compensates for differences in brightness that are a function of elevation and azimuth.

Table 1 outlines the datasets which are presented here. Sources were chosen from the third EGRET catalog (Hartman et al., 1999) and from the GeV catalog (Lamb and Macomb, 1997) based on flux, spectral index and position in the sky; sources chosen away from away from 18^h right ascention are generally given more time on the instrument, due to competition from other observing requests and the onset of the local summer monsoon season.

3 Analysis

Before any analysis is performed, all data are subject to a number of standard operations. The first is to remove an artificially injected pedestal current, which is used to allow the background night sky fluctuation to be characterized. The second is to compensate for any non-uniformities in the camera, a result of small differences in the gains on each tube.

Table 1. Unidentified EGRET sources selected for observation.

	Position				EGRET spectrum		Observation	Exposure
Source	**RA**	**Dec**	**l**	**b**	**Flux[1]**	**Spec. Index**	**dates**	**(min)**
3EG J0423+1707	04:23:00	17:06:60	178.48	-22.14	15.8 ± 2.7	2.43 ± 0.21	2000/12 - 2001/02	248
GeV J0433+2907	04:33:38	29:05:56	170.50	-12.58	22.0 ± 2.8	1.90 ± 0.10	1999/11 - 2000/01	500
3EG J0450+1105	04:50:00	11:05:00	187.86	-20.62	109.5 ± 19.4	2.27 ± 0.16	2000/11 - 2001/01	274
3EG J0634+0521	06:33:12	05:53:07	206.18	-1.41	25.5 ± 5.1	2.03 ± 0.26	2000/11 - 2001/03	275
3EG J1323+2200	13:23:03	21:59:41	359.33	81.15	18.1 ± 4.0	1.86 ± 0.35	2001/01 - 2001/02	83
GeV J1907+0556[2]	19:07:41	05:57:14	40.08	-0.88	62.1 ± 8.9	2.38 ± 0.17	2000/05 - 2000/06	277
GeV J2020+3658[3]	20:20:43	36:58:38	75.29	0.24	59.1 ± 6.2	1.86 ± 0.10	1999/10 - 1999/11	139
3EG J2227+6122	22:27:14	61:22:15	106.53	3.18	41.3 ± 6.1	2.24 ± 0.14	2000/09 - 2000/10	341

[1] Flux from Hartman et al. (1999) for E>100MeV in $10^{-8}\mathrm{cm}^{-2}\mathrm{s}^{-1}$

[2] Roberts et al. (2001) note that this source is over 1° away from 3EG J1903+0550, with which it is associated in Hartman et al. (1999). They conclude that this association is likely to be incorrect.

[3] This source is incorrectly associated with 3EG J2016+3657 in the third EGRET catalog. Roberts et al. (2001) note that 3EG J2021+3716 is consistent with the GeV source.

Artificially generated noise is added to each image to remove any biases that exist between the on-source and control observations, a process referred to as *software padding*. These biases result from the control data being taken while pointing to a different part of the sky which has different background light characteristics. These differences are largest when looking at sources in the galactic plane, when the control run may be in a significantly darker region outside of the plane. Finally, each image is cleaned by ignoring all channels which do not have sufficient signal in them. The details of these procedures are described elsewhere (Reynolds et al., 1993; Cawley et al., 1990)

For extended sources or sources where the source location is not well determined, it is essential to reconstruct the arrival direction of the primary. For a single telescope, such as the Whipple 10m, the arrival direction must be inferred from the "shape" of the single observed image. There are a number of methods available, the approach taken here, described in detail in Lessard et al. (2001), is to assume that the arrival direction of the primary lies along the major axis of the shower image and is displaced from the center of the shower image by a distance given by,

$$disp = \xi \left(1 - \frac{width}{length}\right)$$

where $width$ and $length$ describe the shape of the recorded image and ξ is a scaling parameter.

This method yields two possible arrival directions, each of which is on the major axis of the shower image, seperated from the centroid by the calculated parameter, $disp$. When creating a 2D map the origin of each event is assigned to both possible directions in the hope that one will have an excess as more event origins are superimposed.

A sky map is then produced by building up a 2-dimensional histogram of the reconstructed arrival direction with respect to the center of the camera. Errors in reconstructing both the image axis and $disp$ are accounted for by convolving the final 2D map with a Gaussian function $g(\boldsymbol{r}; r_0) = \exp(-r^2/2r_0^2)$, where r_0 is a scaling parameter chosen to maximise the significance of an excess.

Calculation of excess signal, significance and upper-limit maps ($S(\boldsymbol{r})$, $\sigma(\boldsymbol{r})$ and $UL(\boldsymbol{r})$ respectively) is then done by convolving the ON and OFF counts with the smoothing function $g(\boldsymbol{r})$ in the appropriate manner,

$$S(\boldsymbol{r}) = \sum_{\boldsymbol{r'}} [ON(\boldsymbol{r'}) - OFF(\boldsymbol{r'})] g(\boldsymbol{r'} - \boldsymbol{r})$$

$$\Delta S(\boldsymbol{r})^2 = \sum_{\boldsymbol{r'}} [ON(\boldsymbol{r'}) + OFF(\boldsymbol{r'})] g^2(\boldsymbol{r'} - \boldsymbol{r})$$

Then $\sigma(\boldsymbol{r}) = S(\boldsymbol{r})/\Delta S(\boldsymbol{r})$ and $UL(\boldsymbol{r})$ is calculated from $S(\boldsymbol{r})$ and $\Delta S(\boldsymbol{r})$ by the method of Helene (1983).

4 Calibration

Calibration of the two dimensional analysis method was done using sets of observations of the Crab Nebula. Taking observations with the source location offset from the center of the field of view by various degrees and calculating the relative γ-ray rate allows a model of the detector response for off-axis and extended sources to be made.

Optimizing on the 0.0° offset data, it was found that $\xi = 1.5$ and $r_0 = 0.175^\circ$ gave the highest significance. This is not the value of r_0 that yields the highest angular resolution.

Figure 1 shows significance maps for the Crab Nebula offset by three different amounts. In each of them the Crab is clearly visible. At an offset of 0.3° the γ-ray collection efficiency is 84% of what it is on axis. At an offset of 1.3°, with the source outside of the geometrical extent of the camera, the efficiency is 30%. The significance map for this data shows appreciable background contamination over the field due to the simple reconstruction approach of assigning the arrival direction of each photon to two points on the shower axis. More sophisticated approaches can reduce such false sources (Lessard et al., 2001).

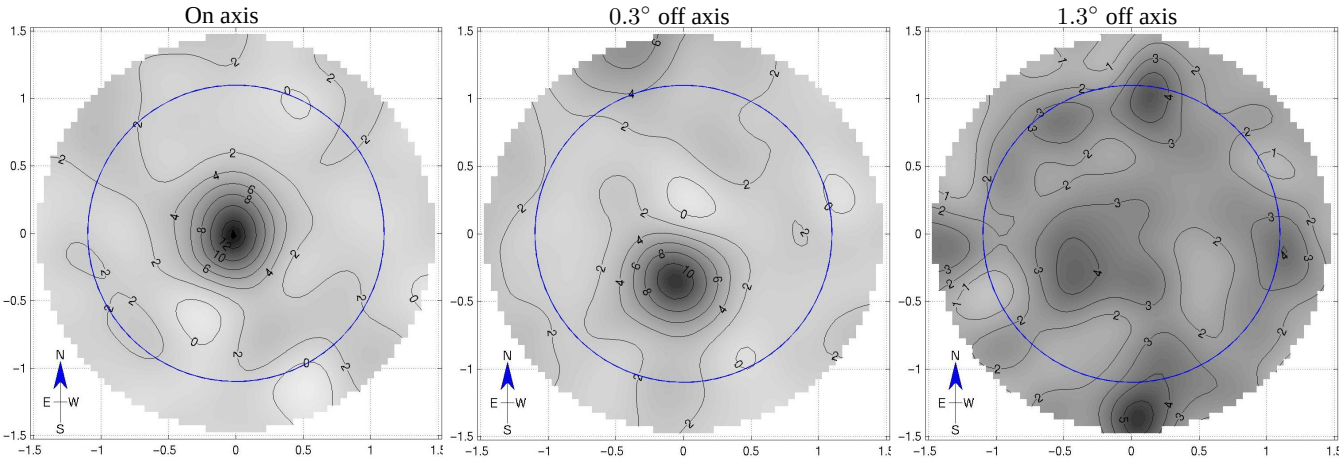

Fig. 1. Observations of the Crab Nebula, offset by varying amounts from the center of the field of view. The contours show detection significance. Positions are in degrees from the center of the field of view with RA and Dec increasing toward the left and top respectively. A circle of radius 1.1° denotes the geometrical extent of the camera used. The observations at an offset of 1.3° place the Crab outside of this.

For data taken during the Fall and Winter 1999-2000 the detection efficiency was lower than during 2000-2001, due to the poorer mirror reflectivity. The Crab rate is taken to be a factor of 0.88 lower during this period and the flux scaled appropriately.

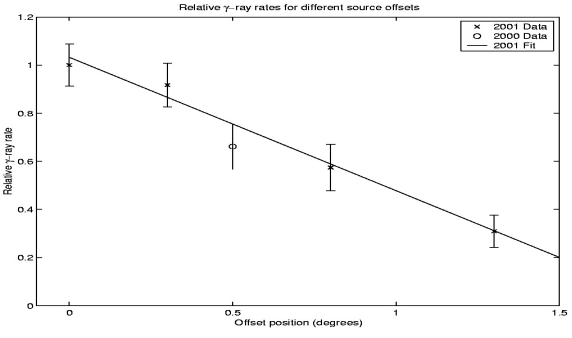

Fig. 2. Relative Crab rate as a function of source offset. The off-axis response can be fit by a straight line.

Figure 2 shows the relative collecting efficiency for offset sources. This curve is used to normalize detected emission rates or upper limits to the Crab flux. It is desirable to fully characterize the response of the instrument to offset sources, i.e. to calculate the energy threshold and collecting area. This has not been done for this work.

5 Results

In one case, GeV J1907+0556, the analysis indicated significant emission throughout the 7 square degree field, the result of large brightness differences between ON and OFF observations that was not fully compensated for in padding. For this source alone, the ON source counts were scaled by a value calculated by examining the number of counts in the region of $1.4^\circ < r < 1.8^\circ$ from the center of the field of view.

Table 2. Upper limits derived from Figure 3.

Source	Positional Error[1] (degrees)	Upper Limit[2] (E >430GeV)
3EG J0423+1707	0.77	3.6
GeV J0433+2907	0.35	2.1
3EG J0450+1105	0.64	3.8
3EG J0634+0521	0.67	2.4
3EG J1323+2200	0.47	5.9
GeV J1907+0556	0.38	2.7
GeV J2020+3658	0.28	4.1
3EG J2227+6122	0.48	2.6

[1] 95% confidence circle from Lamb and Macomb (1997) or Hartman et al. (1999) as appropriate.
[2] Fluxes in units of $10^{-11}\mathrm{cm}^{-2}\mathrm{s}^{-1}$ calculated from measured Crab flux of Hillas et al. (1998).

No significant emission was detected from any source. Figure 3 shows upper limits on emission from the sources observed. Table 2 summarizes these results for the error circle of each object. In each case, the highest limit found in each region is quoted.

Acknowledgements. We acknowledge the technical assistance of K. Harris and E. Roache. This research is supported by the U.S. Department of Energy, PPARC (U.K.) and Enterprise Ireland.

References

Cawley, M.F., et al., Exper. Astr., 1, 173, 1990
Finley, J.P., et al., To appear in these proceedings, 2001
Hartman, R.C., et al., ApJS, 123, 79–202, 1999
Helene, O., NIM, 212, 319, 1983
Hillas, A.M., et al., ApJ, 503, 744, 1998
Lamb, R.C. and Macomb, D.J., ApJ, 488, 872-880, 1997
Lessard, R.W., et al., Astropart. Phys., 15, 1-18, 2001
Ong, R.A., Phys. Rep., 305, 93, 1998
Reynolds, P.T., Akerlof, C.W., Cawley, M.F., ApJ, 404, 206, 1993
Roberts, M.S.E., Romani, R.W., Kawai, N., ApJS, 133, 451, 2001

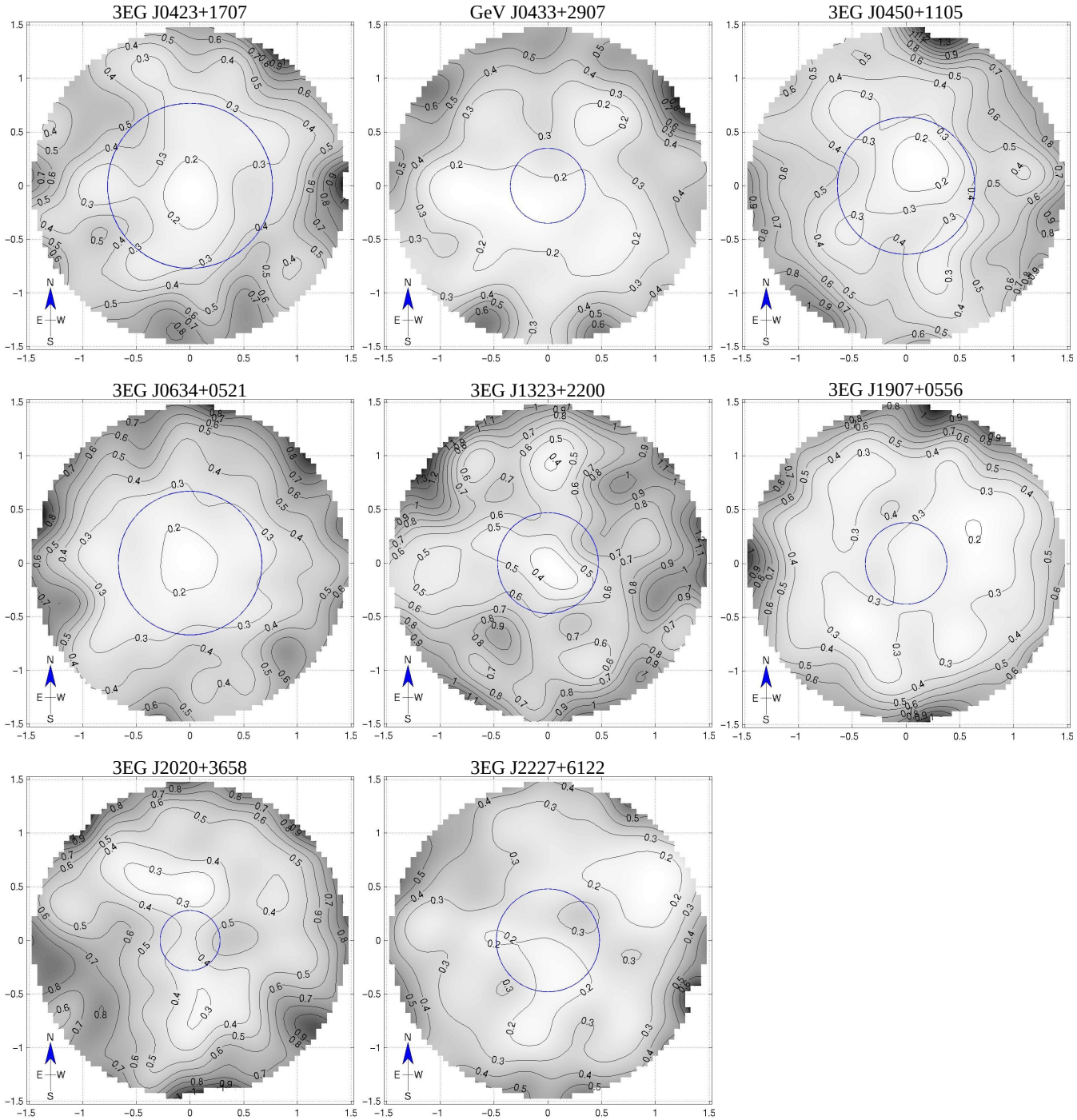

Fig. 3. VHE upper limits on emission. Upper limits are given in units of the Crab Nebula flux. The axes are in degrees from the center of the field of view as given in Table 1. Increasing declination is toward the top of each plot, increasing RA to the left. The circle indicates the 95% confidence circle from Lamb and Macomb (1997) or Hartman et al. (1999) as appropriate. Where error ellipses have been given in in Lamb and Macomb (1997), a circle with radius equal to the semi-major axis is displayed. The maximum upper limit in each 95% confidence region is given in Table 2.